IECON 2022 – 48th Annual Conference of the IEEE Industrial Electronics Society | 978-1-6654-8025-3/22/$31.00 ©2022 IEEE | DOI: 10.1109/IECON49645.2022.9968355

A Carrier-comparison-based Implementation Strategy of A 24-sector-based SVPWM Technique of Asymmetrical Six-phase Machine in Overmodulation Region

Sayan Paul
Department of Electrical Engineering
Indian Institute of Science, Bangalore, India
sayanp@iisc.ac.in

Kaushik Basu
Department of Electrical Engineering
Indian Institute of Science, Bangalore, India
kbasu@iisc.ac.in

***Abstract*—An asymmetrical six-phase machine (ASPM) with two isolated neutral points is analyzed in two orthogonal planes-one of these planes is associated with electromagnetic energy transfer. The energy-transferring plane of ASPM has two regions-linear and overmodulation (OVM). Unlike the linear region, the average voltage injected in the non-energy transferring plane of the OVM region is non-zero. The efficacy of carrier-based implementation of an equivalent space-vector PWM (SVPWM) technique to reduce the computational burden is well-known in three-phase inverter literature. Although carrier-based implementations of popular SVPWM techniques of ASPM are researched for the linear region, such carrier-based implementation doesn't exist for the OVM region. Moreover, a direct extension of the carrier-based strategy in the linear region to the OVM region isn't possible because it requires the calculation of non-zero voltages in the non-energy transferring plane. This paper presents a carrier-based implementation of one of the SVPWM techniques in the OVM region, resulting in minimum RMS harmonic voltage. The proposed technique is a natural extension of an important known PWM technique applied in the linear region. The proposed algorithm generalizes the duty signals in terms of maximum, middle, and minimum of three intermediate signals. These duty signals are then compared with two carrier signals to generate the required gating pulses. The proposed algorithm is validated through simulation and experiment on a hardware prototype at a maximum power of 4.5 kW.**

***Index Terms*—asymmetrical six-phase machine, carrier-based implementation, linear and overmodulation region**

I. Introduction

An asymmetrical six-phase machine (ASPM) is the most common multi-phase machine used for high-power traction drives, safety-critical applications, ship propulsion, aircraft, and electric vehicles, [1]. The vector-space-decomposition-based modeling of ASPM analyse the machine in three two-dimensional orthogonal subspaces, namely, $\alpha-\beta$, z_1-z_2 and o_1-o_2. The $\alpha-\beta$ plane is the only plane responsible for electromagnetic energy transfer, [2]. This plane can be divided into two regions-1) linear region, where no average voltage is applied in the z_1-z_2 plane, [1], [3]; 2) Overmodulation (OVM) region, where harmonic voltages are applied in z_1-z_2 to achieve higher DC-bus utilization. [4], [5] derived the optimal average voltage in z_1-z_2 plane which minimizes the root-mean-square (RMS) of the injected harmonic voltage in z_1-z_2 plane. [4] further proposed eight switching sequences in one part of the OVM region, known as OVM zone-1 (OVMZ1), and two sequences in another part of the OVM region, called OVM zone-2 (OVMZ2). Combining these sequences, $8\times 2=16$ PWM techniques are possible in the entire OVM region.

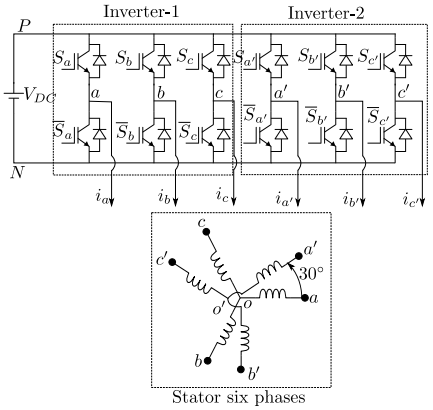

Fig. 1: Six-phase inverter fed ASPM

In a carrier-based implementation, switching signals are generated by comparing the duty ratios with a triangular carrier. Therefore, the objective of any carrier-based PWM scheme is to compute these duty signals from the reference output voltage signals through a reduced number of computation steps. The advantage of the carrier-based implementation of an equivalent space-vector PWM (SVPWM) technique to reduce the computational burden is well-known in three-phase Conventional SVPWM (CSVPWM), [6]. For an ASPM drive, carrier-based implementation implies direct computation of duty cycles from the average $\alpha-\beta$ plane voltages generated by the closed-loop current or torque controller. Carrier-based implementation of the well-known PWM strategies of ASPM in the linear region can be found in [7]–[9]. Such implementation in the OVM region is relatively complex because, unlike the linear region, the average z_1-z_2 plane voltage is non-zero in OVM.

[4] gives the expression of optimized non-zero z_1-z_2 plane voltage as functions of $\alpha-\beta$ plane voltages for one of the twenty-four sectors, known as sector-1. These expressions in the OVM region change from one sector to another. To

obtain these expressions in sectors other than the first sector, the proposed implementation strategy of [4], [5] performs the following operations- i) transform the voltages in $\alpha-\beta$ plane from the given sector to sector-1; ii) calculate z_1-z_2 plane voltages corresponding to sector-1; iii) inverse transform to get the z_1-z_2 plane voltages corresponding to the original sector; iv) apply a 6×6 transformation; and v) then find the duty signals based on modulation signals and common-mode signal. [10] proposed one OVM technique that can be applied only in the OVMZ1 region. But the average voltage applied in the z_1-z_2 plane is not the same as the optimal voltage derived in [4], [5], and hence, the harmonic distortion in the voltage is not minimum in OVM. All the carrier-based implementations of the techniques given in [4], [5], [10] suffer from one major problem- they don't take the switching sequence into account, and that results in applying different kinds of voltage vectors in different sectors of the $\alpha-\beta$ plane.

It is clear from the above discussion that no carrier-based implementation of OVM techniques exists in the literature that applies the optimal average voltage in the z_1-z_2 plane and the same kind of voltage vectors throughout the $\alpha-\beta$ plane. This paper presents the carrier-based implementation of one of the sixteen optimal PWM techniques, as proposed by [4], in the OVM region, which gives the minimum RMS value of the injected harmonic voltage. This technique is the natural extension of the PWM technique proposed by [11] in the linear region, which has superior current-ripple performance. The paper generalizes the aforementioned calculation-intensive step of determining the duty signals in terms of maximum, middle, and minimum of three intermediate modulation variables per three-phase inverter. It also shows that the above generalization only requires the identification of 4 sectors per three-phase inverter instead of 24 sectors. The paper shows that two 180° phase-shifted triangular carriers are required to apply the same type of voltage vectors throughout the OVM region in the $\alpha-\beta$ plane.

The rest of the paper is organized as follows- section-II discusses briefly the technique in linear and OVM region; section-III gives the carrier-based implementation of the technique; section-IV validates the proposed algorithm through experiment and simulation; and the paper is concluded in section-V.

II. The 24-sector-based SVPWM technique

A two-level six-phase (6ϕ) inverter-fed asymmetrical six-phase machine (ASPM) is shown in Fig. 1. ASPM has two sets of balanced three-phase (3ϕ) windings, and the spatial displacement between these two sets is 30° electrical. These two sets of windings have two isolated neutral points, o and o'. The remaining six terminals, .viz, a, b, c, of first set and a', b', c' of the second set, are directly connected to the pole points of two 3ϕ inverters, Inverter-1 and Inverter-2, respectively, as shown in Fig. 1.

TABLE I: Switching States of Three-phase Inverter

S_a	S_b	S_c	Label	S_a	S_b	S_c	Label
OFF	OFF	OFF	0	OFF	ON	ON	4
ON	OFF	OFF	1	OFF	OFF	ON	5
ON	ON	OFF	2	ON	OFF	ON	6
OFF	ON	OFF	3	ON	ON	ON	7

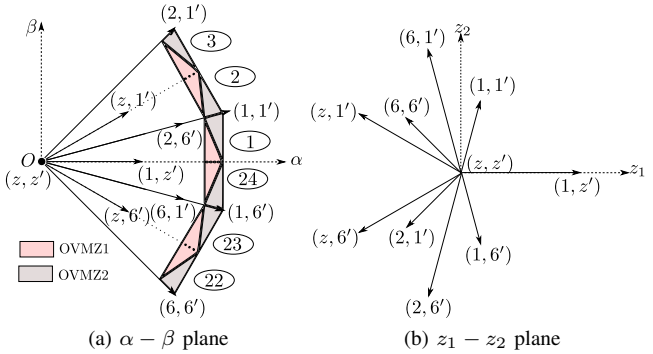

(a) $\alpha-\beta$ plane (b) z_1-z_2 plane

Fig. 2: Mapping of 16 states in $\alpha-\beta$ and z_1-z_2 planes.

A. Modeling of the Converter and ASPM:

The 6ϕ inverter has 64 switching states. These states are labelled by an ordered pair, like, (p,q'), where p and q are the switching states of 3ϕ inverters, Inverter-1 and Inverter-2, respectively, and $p,q\in\{0,1..7\}$. These eight numbers denote the 'ON' or 'OFF' state of the top switches of three legs of the 3ϕ inverter, as shown in Table I. The bottom switches are complementarily switched to top switches with a dead-time. A 6×6 transformation matrix, T, as given in (1), is used to model ASPM and the inverter, [2]. T transforms quantities from original domain to three two-dimensional orthogonal subspaces, namely, $\alpha-\beta$, z_1-z_2 and o_1-o_2. It is possible to show that for a balanced ASPM with two isolated neutral points, as shown in Fig. 1, the instantaneous voltage vector applied by any switching state in the o_1-o_2 plane is zero. Therefore, this plane is not considered for the discussion of modulation. The 64 states of the 6ϕ inverter divide the $\alpha-\beta$ plane into 24 equivalent sectors. For brevity, the mapping of only 16 switching states in $\alpha-\beta$ and z_1-z_2 planes are shown in Fig. 2. These states are adjacent to one of the 24 sectors of $\alpha-\beta$, conventionally known as sector-1. Oval-shaped curves surround the sector numbers in Fig. 2a. z in Fig. 2 denotes the zero-state of 3ϕ inverter, i.e., $z\in\{0,7\}$ of Table I.

$$\begin{bmatrix} x_\alpha \\ x_\beta \\ x_{z_1} \\ x_{z_2} \\ x_{o_1} \\ x_{o_2} \end{bmatrix} \triangleq \underbrace{\frac{1}{\sqrt{3}}\begin{bmatrix} 1 & -\frac{1}{2} & -\frac{1}{2} & \frac{\sqrt{3}}{2} & -\frac{\sqrt{3}}{2} & 0 \\ 0 & \frac{\sqrt{3}}{2} & -\frac{\sqrt{3}}{2} & \frac{1}{2} & \frac{1}{2} & -1 \\ 1 & -\frac{1}{2} & -\frac{1}{2} & -\frac{\sqrt{3}}{2} & \frac{\sqrt{3}}{2} & 0 \\ 0 & -\frac{\sqrt{3}}{2} & \frac{\sqrt{3}}{2} & \frac{1}{2} & \frac{1}{2} & -1 \\ 1 & 1 & 1 & 0 & 0 & 0 \\ 0 & 0 & 0 & 1 & 1 & 1 \end{bmatrix}}_{T} \begin{bmatrix} x_a \\ x_b \\ x_c \\ x_{a'} \\ x_{b'} \\ x_{c'} \end{bmatrix} \tag{1}$$

Modeling ASPM with T shows that the $\alpha-\beta$ plane is solely responsible for electromechanical energy transfer, [2]. The model in the z_1-z_2 plane consists of winding resistance and leakage inductance. Hence, it is not associated with energy transfer. As the impedance offered by the z_1-z_2 plane is low,

TABLE II: Switching sequences in three regions of Sector-1

Region	Sequence	Vector type
Linear	$(0,7')\|(0,6')\|(1,6')\|(1,1')\|(2,1')\|(7,1')\|(7,0')$	3L+2S+2Z
OVMZ1	$(0,6')\|(1,6')\|(1,1')\|(2,1')\|(7,1')$	3L+2S
OVMZ2	$(1,6')\|(1,1')\|(2,1')$	3L

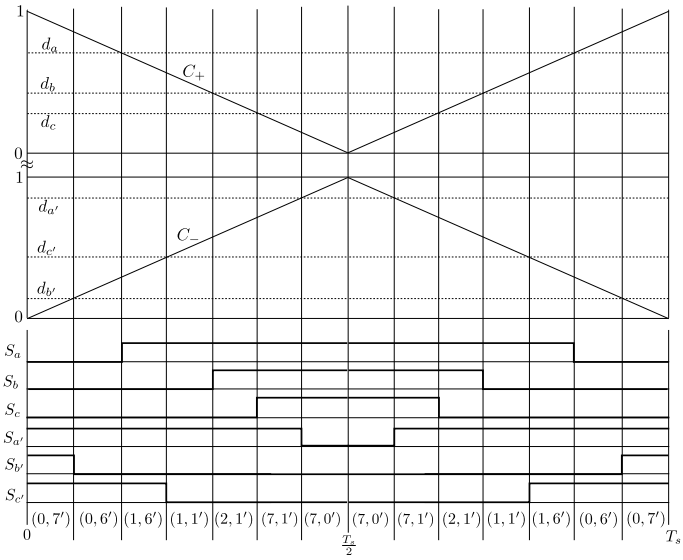

Fig. 3: Carrier-comparison based implementation in sector-1.

PWM techniques should apply an average voltage vector as small as possible in this plane to avoid the resulting unwanted average current and the associated copper loss.

Based on the position of reference voltage vector in $\alpha-\beta$ plane, $\vec{m}_{\alpha\beta} \triangleq m_\alpha + jm_\beta$, the plane is divided in two regions-1) Linear region, where the applied average voltage in $z_1 - z_2$, $\vec{m}_{z_1z_2} \triangleq m_{z_1} + jm_{z_2}$, can be made zero; 2) Overmodulation (OVM) region, where $\vec{m}_{z_1z_2}$ can't be made zero. Here, $m_x, x \in \{\alpha, \beta, z_1, z_2\}$ is the carrier-cycle average voltage in plane x and it is per-unitized with respect to DC-bus voltage, V_{DC}. A brief description of a PWM technique in linear and OVM region follows.

B. A brief discussion of the 24 sector based SVPWM technique in linear and OVM regions

Suppose, $\vec{m}_{\alpha\beta}$ lies in the sector-1. [11] proposed a PWM technique for the linear region that applies the vector sequence as given in the first row of Table II over the half carrier-cycle, $\frac{T_s}{2}$. The remaining half cycle is mirror-symmetric, as shown in Fig. 3. Here, T_s is the carrier period. Therefore, this sequence applies two zero-states (2Z), .viz, $(0,7')$ and $(7,0')$; two small active vectors (2S), .viz, $(0,6')$ and $(7,1')$; and three large active vectors (3L) of $\alpha-\beta$ plane, as shown in Fig. 2a. In short, the sequence is referred as 3L+2S+2Z. According to the proposed scheme of [11], the dwell-times of small and zero vectors are equally divided between its' two redundant states. [1] shows that this PWM technique provides the best current-ripple performance in a significant part of the linear region for an ASPM, whose ratio of high-frequency inductances of $\alpha-\beta$ and z_1-z_2 planes is smaller than 2. For a full-pitched winding machine, this ratio is always less than 2. Therefore, the above PWM technique is of utmost importance.

As discussed earlier, $\vec{m}_{z_1z_2} \neq 0$ in OVM region. The non-zero optimized $\vec{m}_{z_1z_2}$, which gives minimum voltage harmonic distortion in OVM region, is derived in [4]. The expressions for $\vec{m}_{z_1z_2}$ are different in two parts of the OVM region of sector-1. Hence, the OVM region is further subdivided into OVM zone-1 and OVM zone-2, denoted by OVMZ1 and OVMZ2, respectively. Fig. 2a shows linear, OVMZ1, and OVMZ2 regions for $[-45°, 45°]$ of the $\alpha-\beta$ plane, where the inner unshaded part is the linear region. [4] further derived eight sequences in OVMZ1 and two sequences in OVMZ2 of sector-1, which can be used to implement the harmonic-distortion-minimized PWM technique in OVM. Combining these sequences, $8 \times 2 = 16$ PWM techniques are possible in the OVM region. This paper chooses one of these techniques to implement the harmonic-voltage-minimized PWM strategy. The sequences and corresponding vector-types used by this technique in OVMZ1 and OVMZ2 regions of sector-1 over $\frac{T_s}{2}$ are mentioned in the second and third rows of Table II. The two small active vectors (2S states) are applied for an equal duration of time in OVMZ1. Therefore, these sequences are a direct extension of the sequence in the linear region as-i) dwell-time of the zero-vector becomes zero in OVMZ1; ii) dwell-times of both zero-vector and small-vector are zero in OVMZ2, [4].

III. Carrier Comparison Based Implementation

As the gating signals of bottom switches complement the top switches with a fixed dead-time, it is sufficient to discuss the generation of gating pulses only of the top switches. In a carrier-based implementation, gating pulses of the switches are generated by comparing the duty signals with a carrier signal. The output of the speed-torque controller or the input to the PWM modulator of ASPM drive is the voltage in the $\alpha-\beta$ plane. Therefore, for a given $\vec{m}_{\alpha\beta}$, generation of the duty signals and the proper carrier signals to implement the considered SVPWM technique is discussed in this section.

A. Implementation in Sector-1

Fig. 3 shows the gating signals of the top switches of the six legs to generate the 3L+2S+2Z sequence in the linear region of sector-1. The sequences in OVMZ1 (zero-vector dwell-time is zero) and OVMZ2 (zero-vector and small-vector dwell-times are zero), Table II, are two special cases of this sequence.

1) Determination of Duty-ratios: For a two-level 3ϕ inverter with isolated neutral-point, the duty-ratio of the top switch of x-th leg, $d_x, x \in \{a, b, c, a', b', c'\}$, can be written as,

$$d_x = m_x + m_{cm}; \quad d_{x'} = m_{x'} + m'_{cm}; \quad x = a, b, c. \tag{2}$$

Here, m_{cm} and m'_{cm} are the common-mode signals of Inverter-1 and Inverter-2, and they are defined as $m_{cm} \triangleq \frac{v_{oN}}{V_{DC}}$, $m'_{cm} \triangleq \frac{v_{o'N}}{V_{DC}}$. N is the negative DC-bus, as shown in Fig. 1. The modulation signals of the two inverters are defined as $m_x \triangleq \frac{v_{xo}}{V_{DC}}$, and $m_{x'} \triangleq \frac{v_{x'o'}}{V_{DC}}$, $x \in \{a, b, c\}$. The duty signals in (2) have two parts, modulation signals, and common-mode signals, and they are discussed separately below.

***Determination of Modulation Signals**:* In linear region, $m_{z_1} = 0 = m_{z_2}$. The expressions of non-zero $\vec{m}_{z_1z_2}$ in OVMZ1 and OVMZ2 with minimum voltage THD, as derived in [4], [5], are given below as,

$$\vec{m}_{z_1z_2,M} = m_{\alpha,M} - 1 \tag{3a}$$

$$\vec{m}_{z_1z_2,M} = (m_{\alpha,M} - 1) + j\left(2\sqrt{3}m_{\alpha,M} + m_{\beta,M} - (2+\sqrt{3})\right) \tag{3b}$$

These $\vec{m}_{z_1z_2}$ are functions of m_α and m_β. As these expressions are valid only in sector-1 or modulo sector, a subscript M is used for the modulation parameters. Hence in sector-1, $\vec{m}_{z_1z_2,M} = \vec{m}_{z_1z_2}$, $\vec{m}_{\alpha\beta,M} = \vec{m}_{\alpha\beta}$.

To identify the position of $\vec{m}_{\alpha\beta}$ whether in linear or OVMZ1 or OVMZ2 and accordingly choose $\vec{m}_{z_1z_2}$, one needs to check the inequalities, I_1 and I_2, as given below.

$$I_{1,M} : m_{\alpha,M} \leq 1 \tag{4a}$$

$$I_{2,M} : \sqrt{3}m_{\alpha,M} + \frac{m_{\beta,M}}{2} \leq (1 + \frac{\sqrt{3}}{2}) \tag{4b}$$

The subscript M is appended because these inequalities' expression is valid only in sector-1. If I_1 is satisfied, $\vec{m}_{\alpha\beta}$ is in linear region ($\vec{m}_{z_1z_2} = 0$); else in OVM region. Within OVM, if I_2 is satisfied, $\vec{m}_{\alpha\beta}$ is in OVMZ1 ($\vec{m}_{z_1z_2}$ is (3a) in sector-1); otherwise in OVMZ2 ($\vec{m}_{z_1z_2}$ is (3b) in sector-1).

Inverse transformation of (1), i.e., T^{-1} is applied on the given m_α, m_β, and the evaluated m_{z_1} and m_{z_2}, as above, to obtain the modulation signals, $m_x, x \in \{a, b, c, a', b', c'\}$ ($\because m_{o_1} = 0 = m_{o_2}$ for ASPM with two isolate neutrals).

***Determination of Common-mode Signals**:* As discussed earlier, the two zero-states of the 3L+2S+2Z sequence are applied for the same duration of time in the linear region ($(0, 7')$ and $(7, 0')$ in sector-1), [11]. Similarly, the two small active vectors of both 3L+2S+2Z sequence in linear region and 3L+2S sequence in OVMZ1 regions are applied equally ($(0, 6')$ and $(7, 1')$ in sector-1), [4]. Neither 3L state includes the zero-states of any of the two inverters. Therefore, both the inverters apply their corresponding zero states (0, 7 for Inverter-1; $0'$ and $7'$ for Inverter-2) for equal time in linear, OVMZ1 and OVMZ2 regions. Hence, like linear region, [7], the expressions of m_{cm} and m'_{cm} for all three regions can be generalized as,

$$\begin{aligned} m_{cm} &= \frac{1}{2}\left(1 + mid(m_a, m_b, m_c)\right) \\ m'_{cm} &= \frac{1}{2}\left(1 + mid(m_{a'}, m_{b'}, m_{c'})\right) \end{aligned} \tag{5}$$

The mid operator in (5) finds the middle values of the three quantities. Hence, one can determine m_{cm} and m'_{cm} from (5) and subsequently find d_x, (2), from the m_x signals obtained in the previous step, $x \in \{a, b, c, a', b', c'\}$.

2) Choice of Carriers: Once the duty ratios of the top switches are obtained, one needs to use the appropriate carrier to obtain the desired sequence. The gating signal generation logic is as follows: if d_x is greater than the carrier signal, the top switch of the leg is 'ON', i.e., $S_x = 1$; otherwise, $S_x = 0$. Here, $x \in \{a, b, c, a', b', c'\}$. It can be seen from the sequence in sector-1, as shown in Fig. 3, that S_a, S_b and S_c, corresponding to Inverter-1, are 'OFF' at the beginning and end of the carrier-cycle and their non-zero pulses are centred around $\frac{T_s}{2}$. On the contrary, $S_{a'}$, $S_{b'}$ and $S_{c'}$, corresponding to Inverter-2, are 'ON' at the beginning and end of the carrier-cycle and their zero parts are centred around $\frac{T_s}{2}$. Therefore, two 180° phase-shifted unipolar triangular carriers are required to synthesize this sequence, as shown in Fig. 3. Two different labels, C_+ and C_- denote the 'V'-shaped and opposite 'V'-shaped carriers.

B. Implementation in other sectors

1) Determination of Duty-ratios: The same procedure, as discussed for sector-1, can be followed to determine the six modulation signals in other sectors from the given $\vec{m}_{\alpha\beta}$. Note, equation (3) gives the expressions of m_{z_1} and m_{z_2} for OVM region of sector-1 or modulo sector. These expressions change from one sector to another. One needs to follow the below steps to obtain $\vec{m}_{z_1z_2}$ from the given $\vec{m}_{\alpha\beta}$ at OVM of k^{th} sector, [5].

I) Apply (6) on $\vec{m}_{\alpha\beta}$ to get $\vec{m}_{\alpha\beta,M}$. Here, $*$ denotes complex conjugate of the vector.

$$m_{\alpha,M} + jm_{\beta,M} = \begin{cases} \vec{m}_{\alpha\beta}e^{-j\frac{k-1}{2}30^\circ}; k = \text{Odd} \\ \vec{m}^*_{\alpha\beta}e^{j\frac{k}{2}30^\circ}; k = \text{Even} \end{cases} \tag{6}$$

II) Using $m_{\alpha,M}$ and $m_{\beta,M}$, as obtained above, check the inequalities of (4) and determine $\vec{m}_{z_1z_2,M}$ from (3).

III) Apply transformation of (7) on $\vec{m}_{z_1z_2,M}$, as obtained above, to get $\vec{m}_{z_1z_2}$ corresponding to k^{th} sector.

$$\vec{m}_{z_1z_2} = \begin{cases} \vec{m}_{z_1z_2,M}e^{j\frac{k-1}{2}150^\circ}; k = \text{Odd} \\ \vec{m}^*_{z_1z_2,M}e^{j\frac{k}{2}150^\circ}; k = \text{Even} \end{cases} \tag{7}$$

Note, the common-mode expressions, as given in (5), are valid for all the sectors as the dwell times of the zero-vectors of the 3ϕ inverters are split equally between its' two redundant states in all the sectors. Hence, one can now apply T^{-1} on the given $\vec{m}_{\alpha\beta}$ and the $\vec{m}_{z_1z_2}$, obtained from the above steps, to determine m_x, hence, d_x, using (2) and (5).

2) Choice of Carriers: The switching sequences at k^{th} sector, equivalent to 3L+2S+2Z in linear, 3L+2S in OVMZ1, and 3L in OVMZ2, are chosen. Whether the pulses are centered around the middle of the carrier period or start and end of the period, two carrier signals, C_+, or C_-, or both are chosen for the two 3ϕ inverters.

For example, $(0, 0')|(0, 1')|(1, 1')|(1, 6')|(6, 6')|(7, 6')|(7, 7')$ is the equivalent 3L+2S+2Z sequence for sector-24. It can be shown that both the 3ϕ inverters use the same carrier signal to generate this sequence.

TABLE III: Determination of L

Condition	L	$\{d_a, d_b, d_c\}$
$m_{ai} \geq m_{bi} \geq m_{ci}$	1	$\{d_{max}, d_{mid}, d_{min}\}$
$m_{bi} \geq m_{ai} \geq m_{ci}$	2	$\{d_{mid}, d_{max}, d_{min}\}$
$m_{bi} \geq m_{ci} \geq m_{ai}$	3	$\{d_{min}, d_{max}, d_{mid}\}$
$m_{ci} \geq m_{bi} \geq m_{ai}$	4	$\{d_{min}, d_{mid}, d_{max}\}$
$m_{ci} \geq m_{ai} \geq m_{bi}$	5	$\{d_{mid}, d_{min}, d_{max}\}$
$m_{ai} \geq m_{ci} \geq m_{bi}$	6	$\{d_{max}, d_{min}, d_{mid}\}$

C. Generalised Implementation

From the above discussion, it is clear that one needs to identify k to apply the three steps, as described in section-III-B, and find the $\vec{m}_{z_1 z_2}$ in OVM. Here, $k = 1, 2..24$. Identifying these 24 sectors and henceforth application of (6) and (7) in real-time make the implementation calculation intensive. After performing the above three steps to compute $\vec{m}_{z_1 z_2}$ and then finding duty signals (using T^{-1}, (2) and (5)) and carrier signals for all 24 sectors, it is seen that the implementation of the PWM technique can be generalized, as given in the following steps.

1) Determination of Duty-ratios:

- Step-1: Determine six intermediate signals, m_{xi}, $x = a, b, c, a', b', c'$, from the given $\vec{m}_{\alpha\beta}$ as,

$$m_{ai} = \frac{m_\alpha}{\sqrt{3}}; m_{bi} = -\frac{m_\alpha}{2\sqrt{3}} + \frac{m_\beta}{2}; m_{ci} = -m_{ai} - m_{bi} \tag{8a}$$

$$m_{b'i} = -\frac{m_\alpha}{2} + \frac{m_\beta}{2\sqrt{3}}; m_{c'i} = -\frac{m_\beta}{\sqrt{3}}; m_{a'i} = -m_{b'i} - m_{c'i} \tag{8b}$$

  Note, $m_{xi} = m_x$ in the linear region (as $m_{z_1} = 0 = m_{z_2}$), but the same is not true in OVM. The generation of duty signals of Inverter-1 (d_a, d_b, and d_c) from its three intermediate signals, i.e., m_{ai}, m_{bi}, and m_{ci}, are discussed in the remaining steps.
- Step-2: Determine max_i, mid_i, and min_i as follows,

$$\begin{aligned} max_i &= \text{maximum}\{m_{ai}, m_{bi}, m_{ci}\}; \\ mid_i &= \text{middle}\{m_{ai}, m_{bi}, m_{ci}\}; \\ min_i &= \text{minimum}\{m_{ai}, m_{bi}, m_{ci}\} \end{aligned} \tag{9}$$

  During evaluation of (9), one can come up six possibilities as given in first column of Table III and assign the value of L based on the second column of Table III.
- Step-3: Using max_i, mid_i, and min_i, determine the position of $\vec{m}_{\alpha\beta}$ in one of the four generalized sectors, denoted by S1 to S4, using the algorithm shown in flowchart of Fig. 4. Two inequalities, I_1 and I_2, corresponding to each of these generalized sectors (S1 to S4), are given in Table IV. These inequalities are checked to identify the position of $\vec{m}_{\alpha\beta}$ in one of the three regions. If I_1 is satisfied, $\vec{m}_{\alpha\beta}$ is in linear region; else in OVM region. Within OVM, if I_2 is satisfied, $\vec{m}_{\alpha\beta}$ is in OVMZ1; otherwise in OVMZ2.
- Step-4: Based on the position of $\vec{m}_{\alpha\beta}$, three duty ratios, d_{max}, d_{mid}, and d_{min} are calculated using Table V. These duty expressions in linear region are sector-independent.

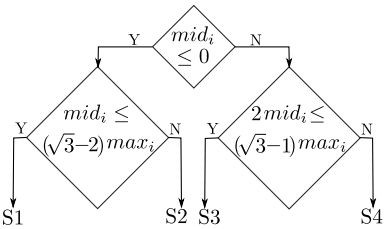

Fig. 4: Flowchart algorithm to identify sectors S1 to S4.

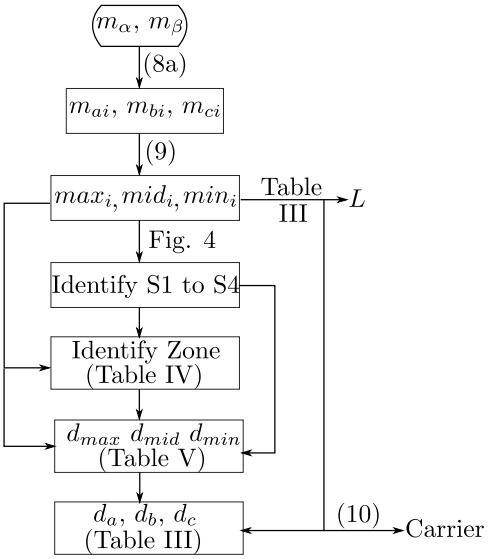

Fig. 5: Flowchart to determine duty signals and carrier of Inverter-1.

- Step-5: Assign these duties to d_a, d_b and d_c using second and third columns of Table III. Note, L was already calculated in Step-2.

2) Choice of Carriers: The generalized formula to choose the carrier is given in (10), where L is already calculated from Table III.

$$\text{Carrier} = \begin{cases} C_+; & L = \text{Odd} \\ C_-; & L = \text{Even} \end{cases} \tag{10}$$

Fig. 5 shows the flowchart to determine the duty signals and carrier signal of Inverter-1 from the given $\vec{m}_{\alpha\beta}$. Following Step-2 to Step-5 and using (10) with respect to intermediate signals $m_{a'i}$, $m_{b'i}$, and $m_{c'i}$, as obtained from (8b), the duty signals of Inverter-2 ($d_{a'}$, $d_{b'}$, $d_{c'}$) and its carrier are obtained.

Table VI compares the computational burdens of evaluating six duty ratios from the given $\vec{m}_{\alpha\beta}$ for the existing implementation strategy of [4], [5] and the proposed strategy. The calculations are shown in terms of comparison (Comp.), assignment (Assign.), multiplication or division (Mul./Div.), addition or subtraction (Add./Sub.), and remainder (Rem.) operations. The existing strategy first finds the sector, k; then applies the three steps of section-III-B to find $\vec{m}_{z_1 z_2}$; and hence applies T^{-1}, (5) and (2) to obtain the duties. Sector identification and application of T^{-1} are two major calculation-intensive steps in the existing strategy which are overcome in the proposed

TABLE IV: Generalised expressions of I_1 and I_2 for zone identification

	S1	S2	S3	S4
I_1	$max_i \leq \frac{1}{\sqrt{3}}$	$max_i - min_i \leq 1$	$max_i - min_i \leq 1$	$-min_i \leq \frac{1}{\sqrt{3}}$
I_2	$3.5max_i + mid_i \leq \frac{2+\sqrt{3}}{2}$	$4max_i + mid_i \leq \frac{2+\sqrt{3}}{\sqrt{3}}$	$max_i - 3min_i \leq \frac{2+\sqrt{3}}{\sqrt{3}}$	$max_i - 2.5min_i \leq \frac{2+\sqrt{3}}{2}$

TABLE V: Generalised duty expressions for S1 to S4, $d_{min} = 1 - d_{max}$

	S1	S2	S3	S4
Linear	$d_{max} = max_i + \frac{mid_i}{2} + \frac{1}{2}$; $d_{mid} = \frac{3mid_i}{2} + \frac{1}{2}$			
OVMZ1	$d_{max} = \frac{7max_i}{4} + \frac{mid_i}{2} + \frac{2-\sqrt{3}}{4}$ $d_{mid} = -\frac{3max_i}{4} + \frac{3mid_i}{2} + \frac{2+\sqrt{3}}{4}$	$d_{max} = 1$; $d_{mid} = \frac{3mid_i}{2} + \frac{1}{2}$		$d_{max} = \frac{7max_i}{4} + \frac{5mid_i}{4} + \frac{2-\sqrt{3}}{4}$ $d_{mid} = \frac{3max_i}{4} + \frac{9mid_i}{4} + \frac{2-\sqrt{3}}{4}$
OVMZ2	$d_{max} = 1$ $d_{mid} = -6max_i + (2+\sqrt{3})$		$d_{max} = 1$ $d_{mid} = -6min_i - (1+\sqrt{3})$	

TABLE VI: Comparison of maximum computational burdens of the proposed and existing implementation strategies

	Comp.	Assign.	Mul./Div.	Add./Sub.	Rem.
Existing, [4], [5]	33	3	54	29	2
Proposed	20	14	18	20	0

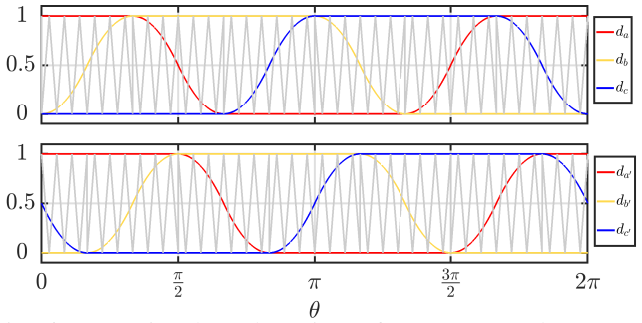

Fig. 6: Duty signals and carriers of Inverter-1 and Inverter-2 at $M_I = 0.622$.

strategy. The reduction in the computational burden of the proposed strategy is evident from Table VI.

If modulation index, M_I, is defined as the ratio between peak of the fundamental line-neutral voltage and V_{DC}, it can be shown that $M_I \in [0, 0.577]$ in linear region and $M_I \in (0.577, 0.622]$ in OVM region, [4]. Fig. 6 shows the duty signals of both 3ϕ inverters along with their carriers at $M_I = 0.622$, obtained after following the above strategy. The top and bottom sub-plots correspond to Inverter-1 and Inverter-2, respectively. It can be seen that the carrier types of both the inverters change after every 60° to the fundamental line cycle.

TABLE VII: Steady-state Circuit Parameters of 6ϕ IM

Per phase stator and rotor resistances	0.675 Ω
Per phase stator and rotor leakage inductances	3.75 mH
Per phase mutual inductance	0.168 H

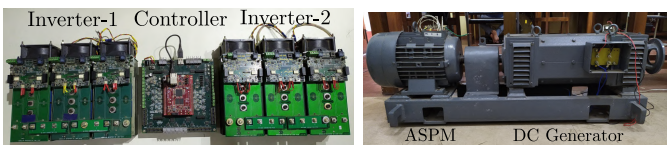

(a) Six-phase inverter and controller (b) ASPM with DC generator

Fig. 7: Experimental set-up

IV. Experimental and Simulation Results

Experiments are performed on a 5 kW, two poles, 120 V line-neutral RMS, 50 Hz asymmetrical six-phase induction machine with squirrel cage rotor to validate the above implementation strategy. Fig. 7b shows the ASPM coupled with a DC generator for loading purposes. The machine parameters are given in Table VII. Fig. 7a shows SKM75GB123D IGBT-based two 3ϕ inverters and a Zynq-7010-based controller card, which are used for the experiment. Simulations are done in MATLAB® Simulink. The operating conditions for experiments and simulations are as follows: $V_{DC} = 275$ V, the carrier frequency of 8.33 kHz, power at $M_I = 0.622$ is 4.5 kW. Experiments and simulations are performed at constant V/f so that at maximum M_I, i.e., 0.622, the line-neutral fundamental voltage is 120 V RMS and frequency is 50 Hz.

Fig. 8a and 8b show the experimental d_a, d_b, $d_{a'}$, and $d_{b'}$ signals over the line-cycle for M_I values of 0.577 and 0.622, respectively. These duty signals are calculated inside the controller and shown in Fig. 8a and 8b through a digital to analog converter (DAC). The waveforms at 0.577 are similar to duty waveforms of conventional SVPWM of 3ϕ inverter. The waveforms at $M_I = 0.622$ match with theoretical waveforms shown in Fig. 6. Fig. 8c, 8d and 8e show the experimental carrier-cycle pole-voltage waveforms for $\vec{m}_{\alpha\beta} \triangleq \sqrt{3} M_I e^{j\theta}$ in linear ($M_I = 0.5$, $\theta = 7.5^\circ$), OVMZ1 ($M_I = 0.59$, $\theta = 7.5^\circ$), and OVMZ2 regions ($M_I = 0.612$, $\theta = 7.5^\circ$) of sector-1. The resulting sequence can be deducted from these waveforms, which are $(0,7')|(0,6')|(1,6')|(1,1')|(2,1')|(7,1')|(7,0')$ (similar to Fig. 3), $(0,6')|(1,6')|(1,1')|(2,1')|(7,1')$, and $(1,6')|(1,1')|(2,1')$, respectively. These sequences are the same as tabulated in Table II. Fig. 8f and 8g show the experimental i_a and $i_{a'}$ waveforms at $M_I = 0.577$ and $M_I = 0.622$, respectively. In the first case, phase currents are harmonics-free, whereas harmonics are present in the second case due to harmonic voltage injection in the $z_1 - z_2$ plane in the OVM region. Fig. 8h shows v_{ab} and $v_{a'b'}$ waveforms at $M_I = 0.622$, which are clamped to positive or negative DC bus for significant part of line-cycle at OVM. As obtained from experiments and simulations, the total harmonic distortion due to the low-frequency harmonic voltages in the OVM region is compared with theoretical plots in Fig. 8i at eleven M_I values between 0.577 and 0.622. The asterisk marks correspond to simulation and experimental

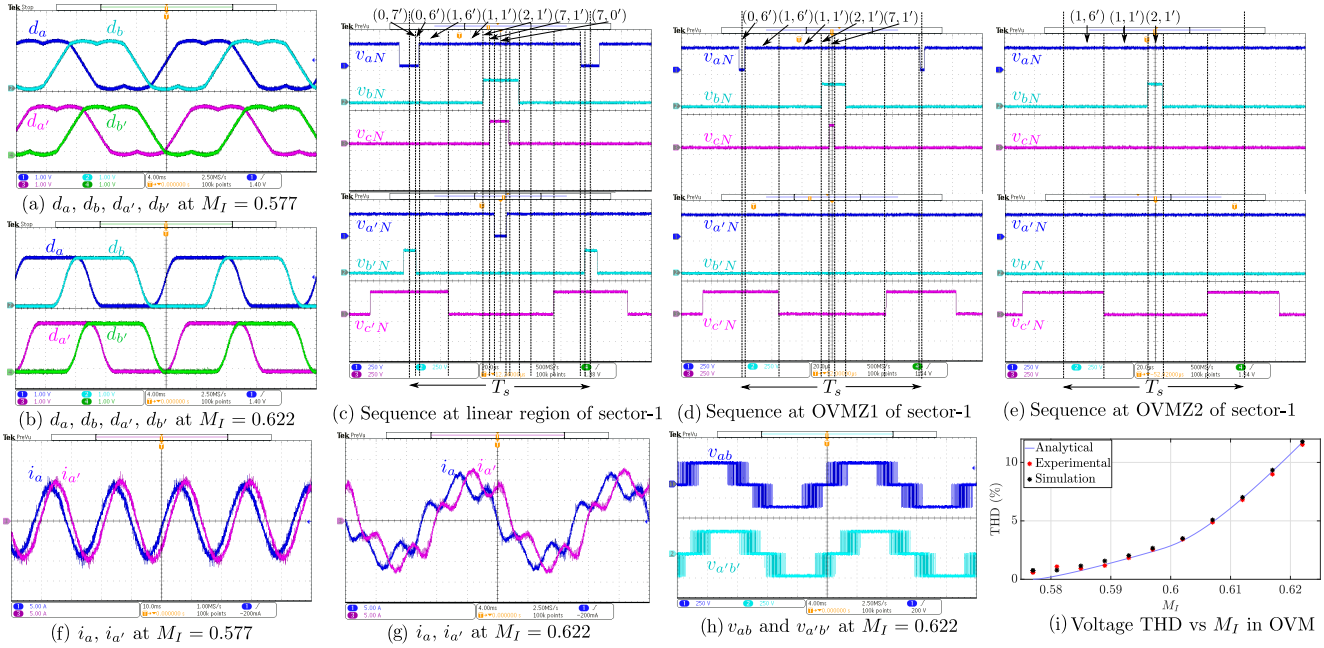

(a) d_a, d_b, $d_{a'}$, $d_{b'}$ at $M_I = 0.577$

(b) d_a, d_b, $d_{a'}$, $d_{b'}$ at $M_I = 0.622$

(c) Sequence at linear region of sector-1

(d) Sequence at OVMZ1 of sector-1

(e) Sequence at OVMZ2 of sector-1

(f) i_a, $i_{a'}$ at $M_I = 0.577$

(g) i_a, $i_{a'}$ at $M_I = 0.622$

(h) v_{ab} and $v_{a'b'}$ at $M_I = 0.622$

(i) Voltage THD vs M_I in OVM

Fig. 8: Experimental waveforms to validate the proposed implementation strategy.

data points, and the continuous line plot is the analytical plot. Harmonics up to 50^{th} order are accounted for in simulated and experimental results to get the THD due to only the low-frequency components and avoid switching frequency components. The theoretical plot corresponds to THD due to the optimal voltage injection in the $z_1 - z_2$ plane, as given in (3) for sector-1. The small but non-zero THD at $M_I = 0.577$ occurs for the dead-time of the inverter or slight asymmetry in the winding, [4]. The close agreements between experimental, simulated, and theoretical results validate the proposed implementation strategy.

V. Conclusion

This paper proposes a carrier-comparison-based implementation strategy of one of the OVM techniques of ASPM, resulting in minimum harmonic voltage injection in the $z_1 - z_2$ plane. The proposed implementation strategy first determines the three intermediate signals per 3ϕ inverters from the given voltages in the $\alpha - \beta$ plane. The four sectors, three zones per sector, and duty expressions in these zones are evaluated using these intermediate signals' maximum, middle, and minimum values. Therefore, the suggested algorithm doesn't require identifying all the 24 sectors and avoiding the calculation-intensive steps, like transformation and inverse transformation of modulation variables to find the non-zero voltages in the $z_1 - z_2$ plane of the OVM region. These duty signals are then compared with two carrier signals, one for each inverter. The algorithm to choose the type of carrier signal is also given in the paper. The correctness of the proposed strategy is validated by experiment and simulation at a 4.5 kW power level.

References

[1] S. Paul and K. Basu, "Linear pwm techniques of asymmetrical six-phase machine with optimal current ripple performance," *IEEE Transactions on Industrial Electronics*, 2022.

[2] Y. Zhao and T. A. Lipo, "Space vector pwm control of dual three-phase induction machine using vector space decomposition," *IEEE Transactions on industry applications*, vol. 31, no. 5, pp. 1100–1109, 1995.

[3] S. Paul and K. Basu, "A new space-vector pwm technique of two-level inverter fed asymmetrical six-phase machine: Analysis and performance evaluation," in *2021 IEEE Energy Conversion Congress and Exposition (ECCE)*, pp. 4796–4802. IEEE, 2021.

[4] S. Paul and K. Basu, "Overmodulation techniques of asymmetrical six-phase machine with optimum harmonic voltage injection," *IEEE Transactions on Industrial Electronics*, vol. 68, no. 6, pp. 4679–4690, 2020.

[5] C. Zhou, G. Yang, and J. Su, "Pwm strategy with minimum harmonic distortion for dual three-phase permanent-magnet synchronous motor drives operating in the overmodulation region," *IEEE Transactions on Power Electronics*, vol. 31, no. 2, pp. 1367–1380, 2016.

[6] V. Blasko, "Analysis of a hybrid pwm based on modified space-vector and triangle-comparison methods," *IEEE Transactions on industry applications*, vol. 33, no. 3, pp. 756–764, 1997.

[7] K. Wang, X. You, and C. Wang, "An equivalent carrier-based implementation of a modified 24-sector svpwm strategy for asymmetrical dual stator induction machines," *Journal of Power Electronics*, vol. 16, no. 4, pp. 1336–1345, 2016.

[8] P. Rakesh and G. Narayanan, "Investigation on zero-sequence signal injection for improved harmonic performance in split-phase induction motor drives," *IEEE Transactions on Industrial Electronics*, vol. 64, no. 4, pp. 2732–2741, 2016.

[9] L. Gopi and G. Narayanan, "Four-dimensional 24-sector svpwm techniques for split-phase induction motor drives: Analysis of modulation process and efficient implementation," in *2022 IEEE International Conference on Power Electronics, Smart Grid, and Renewable Energy (PESGRE)*, pp. 1–6. IEEE, 2022.

[10] S. Paul and K. Basu, "A three-phase inverter based overmodulation strategy of asymmetrical six-phase induction machine," *IEEE Transactions on Power Electronics*, vol. 36, no. 5, pp. 5802–5817, 2020.

[11] C. Wang, K. Wang, and X. You, "Research on synchronized svpwm strategies under low switching frequency for six-phase vsi-fed asymmetrical dual stator induction machine," *IEEE Transactions on Industrial Electronics*, vol. 63, no. 11, pp. 6767–6776, 2016.